Local structure of the crystalline and amorphous states of Ga_2Te_3 phase-change alloy without resonant bonding: A combined x-ray absorption and *ab initio* study

A. V. Kolobov* and P. Fons
Nanoelectronics Research Institute, National Institute of Advanced Industrial Science and Technology (AIST), 1-1-1 Higashi, Tsukuba, Ibaraki 305-8565, Japan
and Japan Synchrotron Radiation Research Institute (JASRI), SPring-8, Mikazuki, Hyogo 679-5198, Japan

M. Krbal
Center of Materials and Nanotechnologies (CEMNAT), Faculty of Chemical Technology, University of Pardubice, Legion's sq. 565, 53002 Pardubice, Czech Republic

K. Mitrofanov and J. Tominaga
Nanoelectronics Research Institute, National Institute of Advanced Industrial Science and Technology (AIST), 1-1-1 Higashi, Tsukuba, Ibaraki 305-8565, Japan

T. Uruga
Japan Synchrotron Radiation Research Institute (JASRI), SPring-8, Mikazuki, Hyogo 679-5198, Japan
(Received 13 October 2016; revised manuscript received 23 January 2017; published 17 February 2017)

Phase-change memories are usually associated with GeTe-Sb_2Te_3 quasibinary alloys, where the large optical contrast between the crystalline and amorphous phases is attributed to the formation of resonant bonds in the crystalline phase, which has a rocksalt-like structure. The recent findings that tetrahedrally bonded Ga_2Te_3 possesses a similarly large property contrast and very low thermal conductivity in the crystalline phase and undergoes low-energy switching [H. Zhu *et al.*, Appl. Phys. Lett. **97**, 083504 (2010); K. Kurosaki *et al.*, Appl. Phys. Lett. **93**, 012101 (2008)] challenge the existing paradigm. In this work we report on the local structure of the crystalline and amorphous phases of Ga_2Te_3 obtained from x-ray absorption measurements and *ab initio* simulations. Based on the obtained results, a model of phase change in Ga_2Te_3 is proposed. We argue that efficient switching in Ga_2Te_3 is due to the presence of primary and secondary bonding in the crystalline phase originating from the high concentration of Ga vacancies, whereas the structural stability of both phases is ensured by polyvalency of Te atoms due to the presence of lone-pair electrons and the formation of like-atom bonds in the amorphous phase.

DOI: 10.1103/PhysRevB.95.054114

I. INTRODUCTION

Nanosecond-order phase transitions in so-called phase-change materials are currently widely used in optical memories such as digital versatile disk random-access memory (DVD-RAM) and also in recently commercialized electronic nonvolatile phase-change random access memory devices (PC-RAM). The basic idea behind phase-change recording is to utilize the optical and/or electronic property contrast between the crystalline and amorphous states, a concept first suggested by Ovshinsky back in the 1960s [1]. The phase-change behavior is usually associated with quasibinary GeTe-based alloys, such as GeTe-Sb_2Te_3 (GST) alloys, of which $Ge_2Sb_2Te_5$ is the best known example. These compounds exhibit very large differences in optical/electronic properties between the crystalline and amorphous phases, high thermal stability of both phases, a fast switching rate, and excellent scalability down to the nanometer-size range, making them ideal materials for storage applications [2,3]. The very low thermal conductivity of the crystalline phase that allows switching of the structure using low-power current pulses is another important attribute of these alloys. This combination of properties is usually attributed to differences in the structure of the amorphous and crystalline phases and, in particular, to the formation of resonant bonds in the crystalline phase as described below.

The amorphous phase of $Ge_2Sb_2Te_5$ has been extensively studied by extended x-ray absorption fine structure (EXAFS) [4–6] and scattering [7] as well as by *ab initio* simulations [8–10] and it was found that the Ge(Sb)-Te bond lengths are equal to the sum of covalent radii suggesting that that bonding in the amorphous phases is purely covalent, although the 8-N rule, established for amorphous semiconductors [11], is not satisfied [9,10,12].

Using an x-ray (Bragg) diffraction analysis, it was concluded that thin amorphous films of quasibinary GeTe-Sb_2Te_3 compositions crystallize into a metastable cubic (rocksalt-like) structure at temperatures around 160 °C [13] and it is this cubic phase of GST that reversibly switches into the amorphous state during the phase-change process. The anion sublattice in the rocksalt-like structure was found to be fully occupied by Te atoms, whereas the cation sites were populated with a composition-dependent random mixture of Ge and Sb atoms and vacancies. The latter were argued to be an intrinsic feature of the crystalline phase [4,14,15]. In order for GST to form the rocksalt structure, all atoms have to be octahedrally (sixfold) coordinated. To satisfy this requirement, the bonding in the

*a.kolobov@aist.go.jp

crystalline state of GeTe and GST has been suggested to be resonant [16,17], with on average one electron per bond.

Subsequent extended x-ray absorption fine structure (EXAFS) studies found that crystallization of these materials resulted in the *elongation* of both Ge-Te and Sb-Te bonds with a concomitant increase in mean-squared relative displacement (MSRD) [4]. These findings are inconsistent with the simple ordering of a covalently bonded solid such as Ge or GaAs where, due to the anharmonicity of the interatomic potential, bonds are shorter and stronger in the crystalline phase [18]. It was also demonstrated that the rocksalt-type structure of GST is distorted; i.e., there are subsets of three shorter and three longer bonds (3+3 coordination), similar to the rhombohedral GeTe, which is one of the end points of these quasibinary alloys. Even the shorter Ge-Te bonds (approximately 2.83 Å), in both GeTe and GST, were found to be significantly longer than the sum of the covalent radii of the participating atoms ($r_{Ge} = 1.22$ Å and $r_{Te} = 1.35$ Å, the total being 2.57 Å) [4]. The presence of the shorter and longer bonds and the associated bonding energy hierarchy [19] suggest that the resonance can only be partial, but this fact does not change the essence of the proposed resonant bonding arguments and in what follows we shall refer to the crystal structure of GST as rocksalt.

Since resonant octahedral bonding in the rocksalt phase requires that the same orbital be used for bonding on two opposite sides of all participating atoms, it was argued that all successful phase-change materials "are characterized by a cubic or near-cubic coordination, which is caused by the dominance of the *p*-electron bonding." It was further argued that tetrahedrally bonded materials are not suitable for phase-change recording, which requires a large optical contrast [20].

The paradigm requiring the existence of resonant bonding between *p*-orbitals in the crystalline phase for a material to be a successful phase-change material has become generally accepted but it has been challenged recently when low-energy switching with very high optical contrast, alongside several other attributes essential for phase-change applications such as the very low thermal conductivity of the crystalline phase, has been reported for tetrahedrally bonded materials such as Ga_2Te_3 [21,22] and Cu_2GeTe_3 [23,24]. In this work, we report the local structure of Ga_2Te_3 obtained from x-ray absorption measurements and *ab initio* simulations and, based on the obtained results, propose a possible atomistic mechanism for the phase-change process in Ga_2Te_3.

II. EXPERIMENTAL AND SIMULATION DETAILS

Bulk Ga_2Te_3, which was subsequently used to fabricate thin Ga_2Te_3 films, was prepared by direct synthesis from stoichiometric amounts of each element (5N purity) placed into a quartz ampoule, evacuated to 10^{-3} Pa, and exposed to a temperature of 1000 °C. The ampoule was allowed to equilibrate for 24 hours, whereupon the furnace temperature was gradually (within 10 hours) lowered to room temperature. Samples for x-ray absorption measurements were prepared on both sides of 15-μm-thick Al foil by pulsed laser deposition (PLD) using the following conditions: a KrF excimer laser (Lambda Physik COMPex 102) operating at 248 nm with a constant output energy of 250 mJ/pulse, a pulse duration of 30 ns, and a repetition rate of 20 Hz. The energy density of the laser beam on the target was 11 J cm^{-2}. The laser beam was directed at a bulk chalcogenide target at an angle of 45°. The target and substrate were rotated, and the distance between them was about 5 cm. The thickness of the deposited thin film of Ga_2Te_3 was ≈1 μm on each side. The composition of the as-grown film was measured by energy-dispersive x-ray spectroscopy and confirmed to be within ±2 at.% of the target composition. Amorphicity of as-deposited samples was confirmed by x-ray diffraction (Fig. 1), the result being in agreement with an earlier study [25], and also by the EXAFS measurements that showed only a first-neighbor correlation for the as-deposited film while higher shells, characteristic of the long-range ordering of the crystalline phase, appeared after annealing [cf. Fig. 4 (lower panel) below].

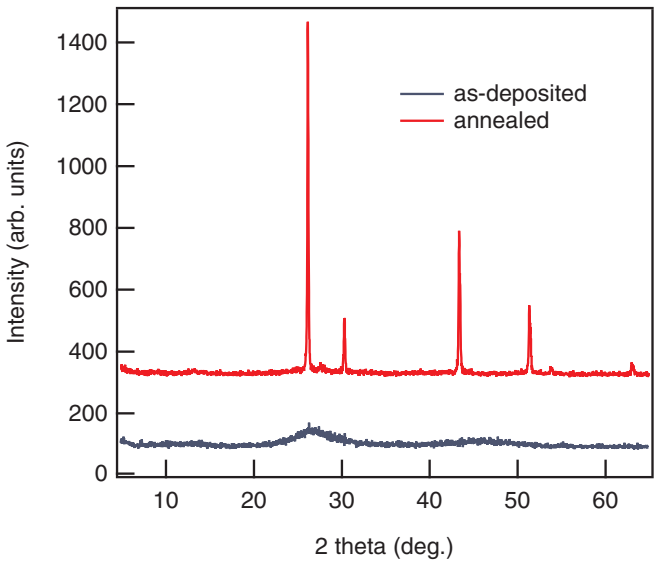

FIG. 1. X-ray diffraction spectra of as-deposited and annealed Ga_2Te_3 films.

A part of the sample was kept amorphous, while the other part was crystallized in a furnace in an inert atmosphere (20 minutes at 450 °C as in Ref. [21]). Based on XRD measurements (Fig. 1), the crystalline film has been identified as Ga_2Te_3 with the lattice parameter of 5.896 Å, which is in perfect agreement with previously reported values ([26] and references therein). The film was then cut into 5 mm × 5 mm squares that were subsequently stacked to obtain optimum edge jumps for x-ray absorption measurements. X-ray absorption spectra, including both the x-ray absorption near-edge structure (XANES) and EXAFS regions, were measured in transmission mode at 8 K at beam line BL01B1 of SPring-8. Analysis of the EXAFS spectra was carried out using the ATHENA and ARTHEMIS packages [27].

Theoretical XANES spectra were calculated using the *ab initio* real-space full multiple-scattering code FEFF9 [28]. FEFF9 is a fully relativistic, all-electron Green's function code that utilizes a Barth-Hedin formulation for the exchange-correlation part of the potential and the Hedin-Lundqvist self-energy correction. In our FEFF calculations, the cluster radius was set to 9 Å around the central atom, which corresponds to about 100 atoms in the cluster. In cases where different local coordinations of Ga and Te atoms were present, the XANES

spectra were calculated for each atom in the unit cell and the obtained spectra were subsequently averaged for comparison with the experimental data.

Ab initio density-functional calculations carried out at 0 K were performed using the plane-wave code VASP [29–31]. PAW pseudopotentials were used for Ga and Te atoms to include the effects of the core electrons [32]. The Ga and Te pseudopotentials explicitly included Ga $3d^{10}4s^24p^1$ and Te $4d^{10}5s^25p^4$ as valence electrons, respectively. The exchange term was evaluated using the generalized gradient approximation (GGA) within the PBE functional [33], both without and with a van der Waals correction. A plane-wave cutoff energy of 295 eV and a $4\times4\times1$ Monkhorst-Pack grid were used. The simultaneous convergence criteria were set to the following values: an energy of 5×10^{-6} eV/atom and maximum force and stress tensor components of 0.01 eV/Å. The melt-quenched structure was generated starting from the crystalline phase by randomizing the structure at 3000 K for 50 ps, followed by linearly cooling the system down to 300 K over a period of 300 ps. A total of 120 atoms were used in an *NVT* ensemble with the density set to a value intermediate between the melt and solid phase. Optical properties were calculated using CASTEP [34] (using the Kubo-Greenwood formula) and the joint densities of states were calculated using OptaDOS [35].

To visualize electron localization two methods are usually used, namely the electron localization function (ELF) [36] and the charge density difference (CDD) [37]. We have chosen to use the CDD approach because it can show using the same basis both the covalent bonds and lone-pair electrons. As the name implies, CDD represents the difference in electron density between atoms in the structure under investigation and isolated quasiatoms. Hence, an appearance of a CDD cloud between two interacting atoms is a signature of a covalent bond [37]. Similarly, a CDD cloud appears at the location of nonbonding lone-pair electrons [38].

III. RESULTS AND DISCUSSION

A. X-ray absorption study

Before we proceed to the description of experimental results and *ab initio* simulations, we note that while crystalline Ga_2Te_3 has a zinc-blende structure ($F\bar{4}3m$ space group) [22], 1/3 of the Ga sites are vacant. In classic semiconductors with a zinc-blende structure such as GaAs both species are fourfold coordinated and out of the four covalent bonds three are conventionally covalent where each participating atom provides one electron per bond, and one bond is dative where both electrons are supplied by the Group V element, such as arsenic. The four bonds, once formed, are indistinguishable and the differences in the source of valence electrons between the conventional covalent and dative bonds is generally ignored. We now consider the unit formula of Ga_2Te_3 as $Ga_2v_1Te_3$, where v stands for a vacancy. In the latter, the two Ga atoms have six unpaired electrons available for conventionally covalent bonding and two empty sp^3 orbitals available for dative bonding. The three Te atoms possess six unpaired electrons to match those of the Ga atoms and additionally have six lone-pair (LP) electrons, located on s and p orbitals. When the Te orbitals become sp^3 hybridized, two of these LPs are used to form two dative bonds utilizing the empty sp^3 orbitals of the Ga atoms and the remaining four form the surrounding of the Ga vacancy. Considering the material's stoichiometry, every Te atom possesses *on average* one nonbonding LP orbital; i.e., despite being sp^3 hybridized they are only *threefold coordinated* (Te^3) in agreement with the experimental EXAFS results. Structural fragments for the ideal zinc-blende structure and Ga_2Te_3 are shown in Fig. 2. In the latter, the LP orbitals are shown as open ovals pointing to a Ga vacancy. When Ga vacancies are perfectly ordered, all Te atoms are threefold coordinated; when vacancies are randomly distributed, in addition to threefold-coordinated Te atoms, twofold-coordinated (Te^2) and fourfold-coordinated (Te^4) atoms are generated in pairs (Fig. 3), reminiscent of valence alternation pairs in chalcogenide glasses [39], whose concentration can easily change if the temperature is high enough to allow for Ga/vacancy diffusion [40–42]. Thus in the example shown in Fig. 3, a single diffusion act of a Ga atom changes a fragment of the structure with seven Te^3 atoms into a structure with a single Te^3 atom and three Te^2Te^4 pairs with the total number of Ga-Te bonds remaining the same. (The positions of the other Ga vacancies, not shown in the figure, are unimportant since the sole goal of the figure is to demonstrate the valency alternation of Te atoms caused by Ga diffusion.) The latter fact suggests that while the structure

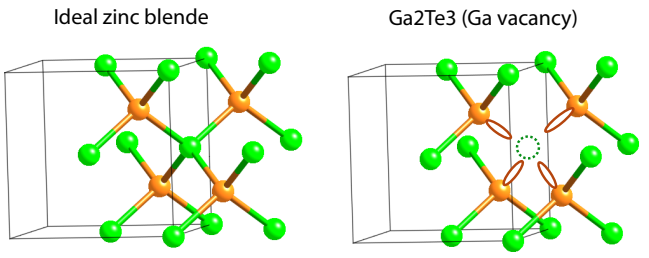

FIG. 2. The ideal zinc-blende structure (left) and a fragment of a structure of Ga_2Te_3 containing a Ga vacancy (right). Ga atoms are shown in green and Te atoms are shown in orange. The oval-shaped unshaded figures depict orbitals with LP electrons.

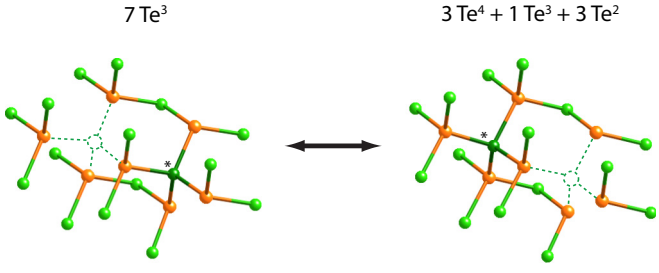

FIG. 3. The effect of Ga diffusion of the coordination of Te atoms. While in the ideal Ga_2Te_3 structure (left panel) all Te atoms are threefold coordinated, a single diffusion act of a Ga atom (marked with an asterisk sign) results in the formation of three Te^2Te^4 valence alternation pairs (right panel). Note that in the shown fragments only those Ga-Te bonds that are formed between the shown atoms are displayed; hence most the Ga species appear to be twofold coordinated.

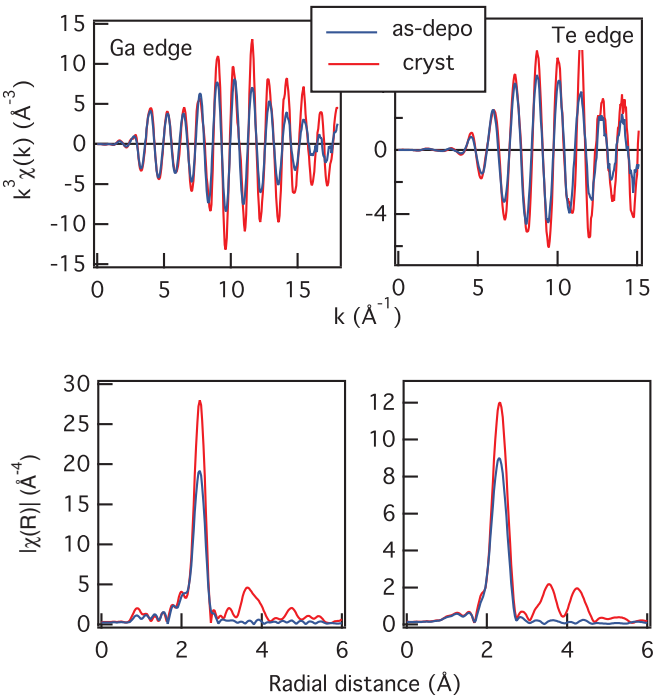

FIG. 4. Raw (upper panel) and Fourier-transformed (FT) (lower panel) χ^3-weighted EXAFS spectra of as-deposited and crystallized Ga_2Te_3 samples measured at the Ga (left) and Te (right) K edges.

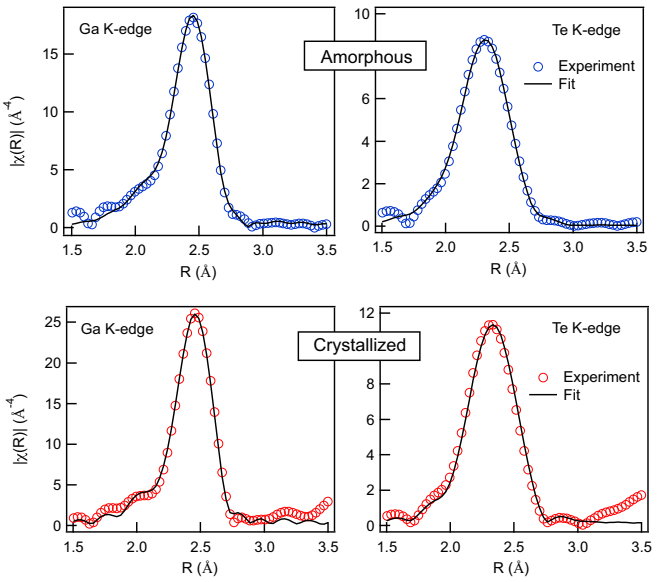

FIG. 5. Real-space fitting of EXAFS data. Upper panel: As-deposited amorphous Ga_2Te_3. Lower panel: Crystallized Ga_2Te_3. The plots on the left are for the Ga K edge and the plots on the right are for the Te K edge.

with an ordered arrangement of vacancies may have the lowest energy, the energy gain is insignificant (up to 0.06 eV per formula unit [43]) and the crystalline phase obtained from the amorphous phase is likely to have a random distribution of vacancies, similar to GST alloys.

Figure 4 compares raw (upper panel) and Fourier-transformed (lower panel) EXAFS spectra for the amorphous and crystalline phases of Ga_2Te_3. Fitting for the first-nearest neighbors was performed using a k range of up to 19 Å^{-1} at the Ga K edge and up to 15 Å^{-1} at the Te K edge. The fitting results are shown in Fig. 5 and the obtained numerical values are summarized in Table I. The obtained bond lengths are in agreement with those reported from earlier EXAFS measurements of amorphous Ga_2Te_3 [25] and longer than those reported for $Ga_2(Se_{0.33}Te_{0.67})_3$ [42]. Since the details of the EXAFS analysis in [42] were not presented, it is not clear what may be the reason for the shorter bonds observed in the cited work.

In both crystalline and amorphous phases a non-negligible concentration of Ga-Ga bonds was detected, while the inclusion of Te-Te bonds did not improve the quality of the fit. One can see that the (total) coordination numbers for both Te (approximately 3) and Ga (approximately 4) species as well as the corresponding bond lengths remain essentially unchanged upon crystallization, which is in contrast to $Ge_2Sb_2Te_5$, where pronounced bond elongation upon crystallization was observed [4]. The Te coordination number in the crystalline phase is significantly lower than four, a value one would normally expect for a zinc-blende structure, but this value is not totally unexpected considering the stoichiometry of the material.

The parameter most affected by crystallization is the mean-squared relative displacement (MSRD), which reflects the increased local order upon crystallization. At the same time, it should be noted that even for the crystalline phase the obtained MSRD value (0.0034 Å^2) is notably larger than for typical tetrahedrally bonded binary semiconductors (e.g., the MSRD of GaAs is about 0.002 Å^2 in this temperature range [44,45]), which suggests rather large static disorder in the structure.

It is interesting to note that while the Ga-edge FT-EXAFS spectrum is characterized by a single second-nearest-neighbor peak in agreement with the proposed zinc-blende structure, the second-nearest-neighbor feature in the Te-edge spectrum is clearly split into two peaks suggesting two different Te-Te distances. The origin of this splitting will be discussed below.

In Fig. 6 we show the measured XANES spectra for the amorphous and crystalline phases at both edges. The changes in the spectra are rather small (compared for example to the

TABLE I. Summary of EXAFS fitting results. CN, coordination number; BL, bond length. The uncertainties for the coordination numbers are ±20%.

Sample	CN_{Ga-Te}	CN_{Ga-Ga}	CN_{Ga}^{total}	CN_{Te}^{total}	BL_{Ga-Te} (Å)	BL_{Ga-Ga} (Å)	MSRD (Å^{-2})
As-deposited	3.79	0.21	4.00	3.28	2.65	2.46	0.0051
Crystallized	3.55	0.20	3.75	3.04	2.65	2.47	0.0034

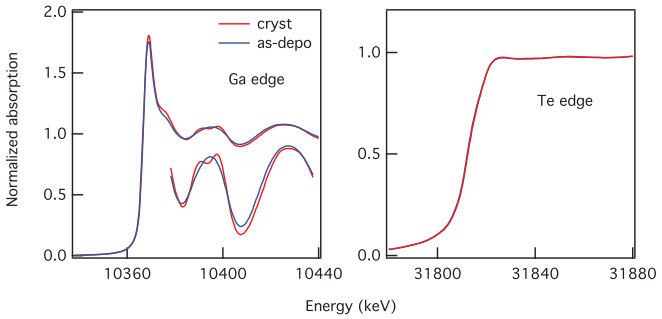

FIG. 6. XANES spectra of as-deposited and crystallized Ga_2Te_3 samples measured at the Ga (left) and Te (right) K edges. The lower curve in the left panel shows a zoomed-in XANES spectrum.

corresponding changes in GST [4]) and suggest that the short- and medium-range order is essentially unchanged in the two phases.

B. *Ab initio* simulations

To obtain further insights into the structural transformations occurring during the phase-change process, we have additionally performed *ab initio* simulations. The results of these studies are reported below starting with the crystalline phase.

The structure of crystalline Ga_2Te_3 for *ab initio* simulations was generated from the ideal zinc-blende structure with GaTe (1:1) stoichiometry and lattice constant of 5.896 Å (the experimental value obtained on our samples) by randomly removing 1/3 of the Ga atoms and subsequently relaxing the structure at 0 K. The relaxed structure and the distribution of Te and Ga coordination numbers and Ga-Te distances are shown in Figs. 7 (upper panel) and 8 (right panel), respectively. The obtained lattice parameter of 6.09 Å is slightly larger than the value obtained in [26], where the band gap of Ga_2Te_3 and related crystals was studied in detail, and also with the reported experimental values of 5.87–5.91 Å ([26] and references therein). Interestingly, the relaxed lattice constant decreased to 5.93 Å, i.e., approached the experimental value, when van der Waals correction was used in the simulation. One can see that the majority of Ga and Te atoms possess the coordination numbers of $N_{Ga} = 4$ and $N_{Te} = 3$, in agreement with the experimental EXAFS results, while a noticeable concentration of twofold-coordinated and fourfold-coordinated Te species is also present. The latter are expected in a structure with a random distribution of Ga vacancies, as discussed above. The Ga-Te first-neighbor distances have a large spread from 2.56 Å to 2.80 Å, which is very similar to the case of amorphous Ga_2Te_3 (Fig. 7) and in agreement with the very large value of MSRD observed experimentally. The Ga-Te-Ga bonding angle (not shown) decreases from 109° in the ideal zinc-blende structure to approximately 105° for those Te atoms that surround a Ga vacancy. The smaller valence angles suggest that the hybridization is incomplete. The charge-density difference (CDD) clouds associated with LP orbitals pointing to a Ga vacancy are clearly visible for Te atoms surrounding Ga vacancies (inset to Fig. 7, upper panel).

It is of special interest that the Te-Te distances between the Te atoms that form a tetrahedron around a Ga vacancy

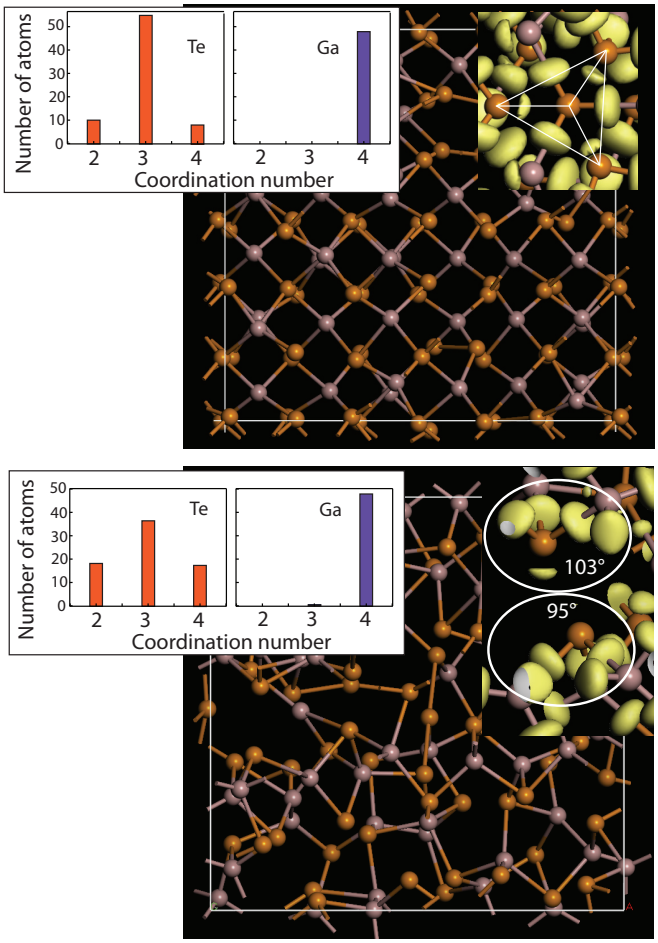

FIG. 7. The DFT-relaxed crystalline phase (upper panel) and a "melt-quenched" amorphous phase (lower panel) of Ga_2Te_3. Te atoms are orange and Ga atoms are violet. The left insets show the distribution of Ga and Te atoms with different coordination numbers. The right insets show CDD isosurfaces. One can see that in the crystalline phase the four Te atoms surrounding a vacancy all possess CDD clouds associated with LP electrons pointing into the center of the vacancy. At the same time, in the amorphous phase, only atoms with larger valence angles have visible CDD clouds; for those atoms that have smaller bonding angles, the CDD cloud disappears, which is attributed to deepening of the LP electrons from the sp^3 orbital into the s-orbital energy levels.

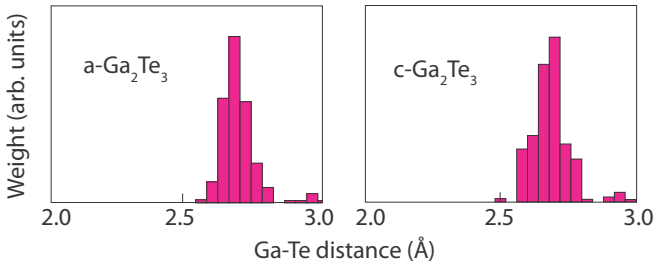

FIG. 8. Comparison of the Ga-Te first-nearest-neighbor bond length distribution in the amorphous (left) and crystalline (right) phases of Ga_2Te_3 (DFT-relaxed at 0 K) demonstrating the very similar widths of the distribution for the two phases.

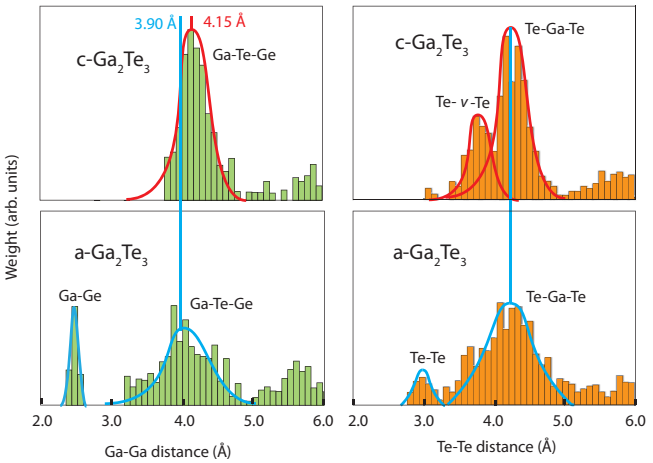

FIG. 9. Distributions of Ga-Ga (left) and Te-Te (right) distances for crystalline (top) and amorphous (bottom) Ga_2Te_3 models shown in Fig. 7.

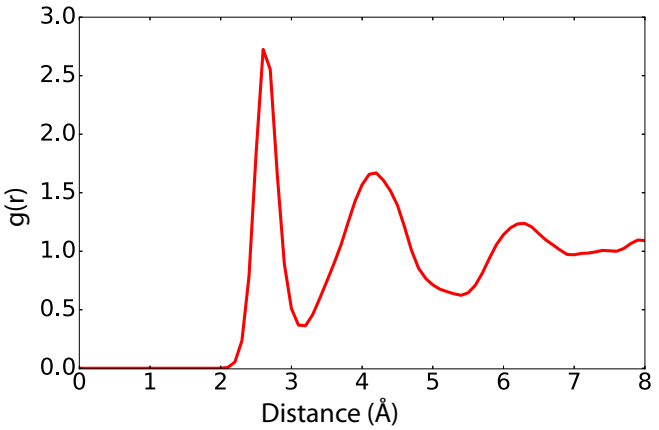

FIG. 10. Radial distribution function for the amorphous phase.

in Ga_2Te_3 drastically decrease from 4.17 Å in the ideal zinc-blende structure to about 3.6 Å in the relaxed structure (Fig. 9, upper right panel), demonstrating that despite the fact that double-filled lone-pair orbitals are involved, there is a pronounced attractive interaction between them. This interaction is somewhat similar to the back-lobe interaction in p-orbital bonded GeTe-based alloys, where it is usually referred to as resonant. Since true resonance in this case is not possible, we shall refer to this interaction as secondary. We further note that this Te-Te distance is similar to the Te-Te distance across the van der Waals gap in layered chalcogenides such as Sb_2Te_3 or $MoTe_2$, where the Te atoms are also spatially arranged to form a pyramid, which suggests that the forces holding the crystalline Ga_2Te_3 phase together also have a dispersive component, i.e., are much weaker than the Ga-Te covalent bonds that form the backbone structure. The obtained better agreement of the simulated lattice constant with experiment upon inclusion of van der Waals correction is also in agreement with this suggestion.

Figure 9 shows the distribution of like-atom distances for the crystalline and amorphous phases. It is of interest to note that while the Ga-(Te)-Ga distances in c-Ga_2Te_3 have a single-peak distribution, the Te-Te correlations are characterized by a bimodal distribution, with the longer distances corresponding to Te-Ga-Te fragments and the shorter distances being due to Te-v-Te atoms, i.e., Te atoms surrounding Ga vacancies, which accounts for the double-peak feature in the FT EXAFS spectrum measured at the Te edge (cf. Fig. 4, lower left panel).

We now proceed to the melt-quenched amorphous Ga_2Te_3 phase obtained through molecular dynamics simulations, which is shown in Fig. 7 (lower panel). Since the sum of Ga and Te covalent radii is ≈2.7 Å, we used the 3.2 Å value as a cutoff distance to visualize the Ga-Te bonds (based on the Lindemann criterion). The obtained radial distribution function (Fig. 10) is typical for an amorphous material.

From Fig. 9, where the distributions of Ga-Ga and Te-Te distances for the crystalline and amorphous phases of Ga_2Te_3 are shown, several observations can be made. The first one is the formation of like-atom (or "wrong") Ga-Ga and Te-Te bonds in the amorphous phase as evidenced by the appearance of peaks centered around 2.5 Å and 2.9 Å, in the left and right lower panels, respectively. The concentrations of the Ga-Ga and Te-Te bonds were found to be rather similar. The second observation is that in the amorphous phase, the 3.7 Å peak corresponding to Te-v-Te fragments essentially disappears indicating the destruction of Te-Te secondary interaction. Finally, one can see that while the (Te-Ga-Te) distance does not change between the two phases, indicating the preservation of the Te-Ga-Te bonding angles, the Ga-Te-Ga second-nearest-neighbor distances become shorter, changing on average from from 4.15 Å to 3.90 Å. This change in the Ga-Te-Ga second-neighbor distance corresponds to a decrease in the average Ga-Te-Ga bonding angle from 105° to 93° and suggests that Te atoms in the amorphous phase are not sp^3 hybridized but essentially preserve their atomic p orbitals. In line with this are the obtained bond-angle distributions (Fig. 11). While for Ga species the distribution peaks around 109° and is symmetric demonstrating the preserved tetrahedral coordination, that for Te atoms is shifted to angles around 90°−100°, a value characteristic of p-orbital σ bonds.

At the same time, a significant fraction of Te atoms (about 50%) acquire twofold (Te^2) and fourfold (Te^4) coordinations. We note here that this change in the Te coordination does not effect the *average* coordination number, which remains $N_{Te} \approx 3$, in agreement with the experimental EXAFS results.

We note here that despite the appearance of Te-Te bonds in the melt-quenched amorphous phase in our *ab initio* simulations, there were no such bonds experimentally detected by EXAFS in as-deposited amorphous films. While this difference may reflect differences in the structure of

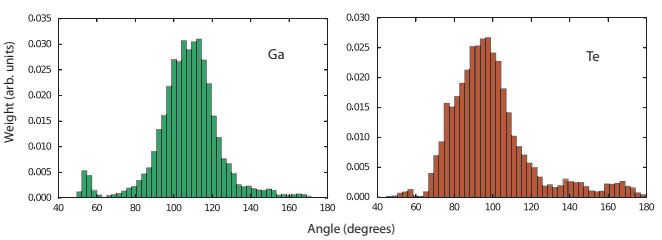

FIG. 11. Bond-angle distributions around the Ga (left) and Te (right) atoms in the amorphous phase.

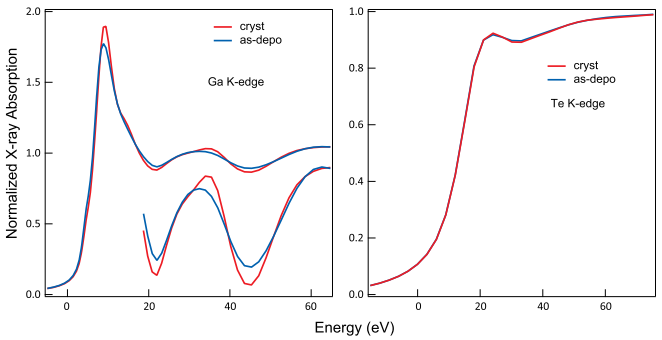

FIG. 12. Simulated XANES spectra for the amorphous and crystalline phases of Ga_2Te_3 at the Ga and Te K edges.

PLD-deposited and computer-generated "melt-quenched" amorphous phases, it may also be a general feature of not detecting small concentrations of Te-Te bonds. Thus a very similar situation was observed for GST alloys, where both Ge-Ge and Te-Te bonds were observed by *ab initio* simulations [8,9] but only Ge-Ge bonds were detected in as-deposited films by EXAFS [6].

In Fig. 12 simulated XANES spectra at the Ga and Te K edges are shown, where the differences between the XANES spectra of the amorphous and crystalline phases at the Ga K edge observed experimentally (cf. Fig. 6) are fairly well reproduced by simulations using an *in silico* generated amorphous phase. The differences between the Te-edge spectra are much smaller, also in agreement with experiment.

Figure 13 compares the optical properties of the crystalline and amorphous phases of Ga_2Te_3 simulated for the structures shown in Fig. 7. One can see that there is a noticeable optical contrast, although it varies significantly with the photon energy. It is interesting to note that the band gap increases for the amorphous phase (similarly to the case of GST), while typically for covalently bonded materials the band gap in the amorphous phase is smaller due to the appearance of localized tail states. The simulated values generally agree with those obtained from ellipsometry measurements although direct comparison of the simulated results with experiment is rather complicated. For the crystalline phase, only the band gap has been reported, the reported values being in the 0.95 eV to 1.38 eV range [21,46–50], which is a disturbingly large range for a crystalline material of nominally the same composition.

For the amorphous phase, a band gap of 1.15 to 1.2 eV has been reported [51,52]. The n and k values have also been obtained for the bulk phase [51] using ellipsometry and for thin films based on transmission measurements [52]. At the same time it should be noted that the bulk amorphous phase studied in [51] was prepared by heating the ampoule (filled with stoichiometric amounts of pure elements) above the melting point, equilibrating for 24 hours, and "slowly lowering the furnace temperature to room temperature (ca. 0.5°/h)" [51]. Since Ga_2Te_3 is not a good glass former and no evidence was presented that the obtained material was amorphous, there is a good chance that what was actually obtained (and studied) was a polycrystalline phase. It should be also noted that Ga_2Te_3 rather easily oxidizes in air [49] and since ellipsometry is a surface-sensitive technique the presence of an uncontrollable oxide layer could have also affected the numerical values [47,49].

In [21], thin-film samples in both amorphous and crystalline states were studied using diffuse reflectance spectroscopy. The details of the sample preparation are not described but oxidation could also have occurred, especially for the crystallized films, considering the tendency of Ga_2Te_3 to oxidize easily, the relatively high crystallization temperature, and the rather poor vacuum used. This may be the reason why the obtained value of the gap (1.38 eV) is higher than the values reported earlier. In order to perform proper comparison, additional experiments are needed.

Since the optical contrast between the two phases may arise from either a change in the joint density of states (JDOS) or matrix elements, it is interesting to disentangle these contributions. In Fig. 14 we show the JDOS for the crystalline and amorphous phases. From a comparison of the shown results, one can see that the JDOSs essentially coincide for the two phases in the energy range of interest, which suggests that the major source of the optical contrast arises from differences in the transition matrix elements, similar to the case of GST [53], where a change in the transition matrix elements is also the dominant factor.

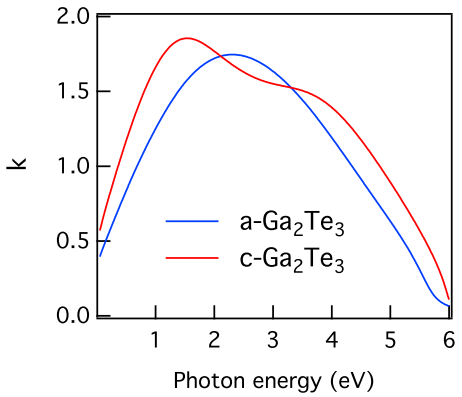

FIG. 13. Refrative indices (k) for the amorphous and crystalline phases of Ga_2Te_3 obtained for the structures shown in Fig. 7.

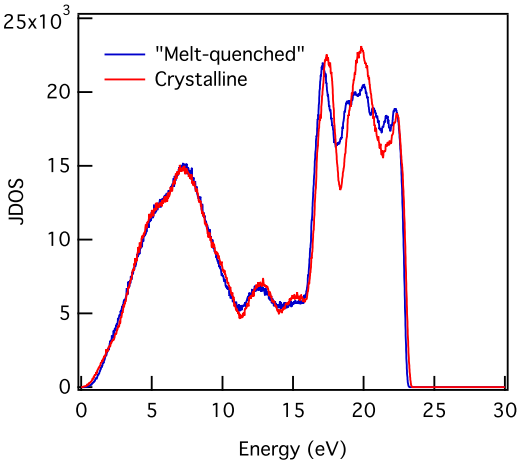

FIG. 14. JDOS of the melt-quenched and amorphous phases of Ga_2Te_3.

C. Mechanism of phase change

For GST alloys, it was argued that exposure to an intense pulse results in the rupture of the longer resonant bonds (referred to as secondary in this work), which leads to the formation of pyramidal Ge configurations, subsequent relaxation of which generates an amorphous phase consisting of both pyramidal (defective octahedral) and tetrahedral configurations [8,54]. Destruction of the "resonant" bonds also results in a significant change of the optical constants [17,19,55].

An essentially similar phase change mechanism can be imagined for Ga_2Te_3. In the crystalline phase, due to long-range forces a zinc-blende-like structure is established with a large concentration of intrinsic vacancies. Te atoms in this structure are sp^3 hybridized but with only three out of four sp^3 orbitals used for covalent bonding. The stability of the zinc-blende phase is ensured by the secondary Te-Te interaction across vacancies. When the structure is excited (thermally or electronically) and atoms are displaced, the secondary Te-Te bonds break and the long-range order is lost, but the short-range *atomic* structure with pyramidal Te-Ga_3 fragments having a Te atom at the apex remains essentially unchanged. This ability to lose the long-range order without rupture of strong covalent bonds—being very similar to the case of GST—is the basis of the phase transformation requiring very little energy.

Of special interest is the formation of Te^2Te^4 pairs in the amorphous phase. When the system is destabilized at higher temperatures (not necessarily by melting) by breaking the secondary Te-Te bonds and atomic diffusion increases, diffusion of Ga atoms from the energetically most stable positions into the neighboring vacancies leads to an increased concentration of Te^2Te^4 pairs. We believe that this change in the Te coordination number, alongside the formation of a small amount of like-atom bonds, is the origin of the observed optical contrast, while the like-atom bonds serve to enhance the stability of the amorphous phase, similarly to the case of GST alloys.

During crystallization, once the few existing like-atoms bonds annihilate, the structure containing exclusively Ga-Te bonds only has to rearrange the atomic position without any further bond reconstruction, which accounts for the experimentally observed energy efficiency of the phase-change process. The process is similar to ordering of ABAB building blocks (square rings) in GST [9,10].

D. Similarities between Ga_2Te_3 and GST alloys

Despite apparently large differences in the bonding character, the two classes of materials share a surprisingly large number of common features, which are discussed below.

We start by noting that both GST and Ga_2Te_3 initially crystallize into a metastable "cubic" phase. In both cases, the metastable structures contain a large concentration of intrinsic vacancies [4,13,14]. Their presence results in significant lattice relaxation with very broad distributions of the bond lengths for the first-nearest neighbors. It is also interesting to note that the ordering of vacancies in the cation sublattice subsequently transforms both structures into the stable hexagonal phase [13,14,56]. For more details on the structure and properties of the stable hexagonal phase of GST the interested reader is referred to [57–59].

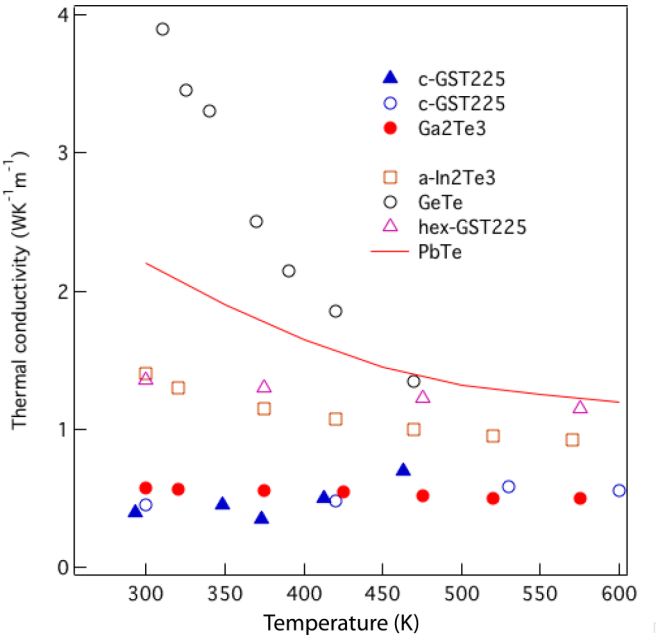

FIG. 15. Temperature dependencies of thermal conductivity in several tellurides. While crystals typically exhibit relatively large values of thermal conductivities that decrease with temperature, both $Ge_2Sb_2Te_5$ and Ga_2Te_3 are characterized by glasslike thermal conductivity (low values and a slight increase with temperature). The shown data are for polycrystalline materials and taken from the sources cited in the main text.

Another common attribute of the crystalline phase is the presence of a bonding energy hierarchy. In GST this refers to the shorter and longer bonds, often referred to as resonant bonds, while in Ga_2Te_3 the weaker secondary bonds are between Te atoms surrounding Ga vacancies. We believe that this common feature is crucial for the efficient phase-change performance in these materials.

We now address another property shared by GST and Ga_2Te_3 that is crucial for an efficient phase-change process, namely the very low values of thermal conductivities. Figure 15 summarizes the lattice thermal conductivities for several resonantly bonded phase-change (and some related) materials. In particular, one can see that while the thermal conductivity of crystalline GeTe [60] (also PbTe [61]), hexagonal $Ge_2Sb_2Te_5$ [62], and α-In_2Te_3 [22] decreases with temperature, i.e., behaves "normally" for a crystal, those for cubic $Ge_2Sb_2Te_5$ [62,63] and Ga_2Te_3 [22] have a glasslike shape (nearly constant with temperature) and the absolute values are very close to those of the amorphous phase. The shown behavior for cubic $Ge_2Sb_2Te_5$ is typical for the whole family of GST alloys [64–66]. In particular, it was reported that low temperature measurements down to 50 K for rocksalt structure $Ge_1Sb_2Te_4$ reveal a glasslike thermal conductivity close to the theoretical minimum for disordered crystals and annealing enhances κ and results in more crystal-like behavior. At the same time, the observed very low value of thermal conductivity in Ga_2Te_3 [22] is rather unexpected because tetrahedrally bonded (diamond-like) solids are usually among the best

thermal conductors [67,68]. Even more interesting is that in both cases the thermal conductivities do not decrease with temperature, a behavior unusual for crystals and characteristic of amorphous solids. Materials exhibiting this kind of behavior are often called "phonon-glass electron-crystals" [69]. We argue that this behavior is due to the presence of a large concentration of intrinsic vacancies and nonbonding LP orbitals that act as highly efficient phonon scatterers in the crystalline structures of these materials that are characterized by very large amorphous-like atomic disorder. The important role of LP electrons in minimizing thermal conductivity was also proposed in [70,71].

Finally, there is another phenomenon common to $Ge_2Sb_2Te_5$ and Ga_2Te_3 and not typically observed in covalently bonded crystals. Namely, upon application of hydrostatic pressure the "cubic" GST phase exhibits loss of long-range order. The pressure at which the amorphization takes place decreases for compositions with a higher concentration of vacancies. At the same time, the vacancy-free trigonal phase of GST and the binary GeTe material do not amorphize [72] demonstrating a clear correlation between pressure-induced amorphization and the presence of vacancies. Subsequent *ab initio* simulations confirmed that the pressure-induced amorphization of cubic GST is associated with drastic structural relaxation around vacancies leading to the destruction of the weaker bonds [73]. A similar result was reported for $AgSbTe_2$; the latter becomes amorphous at pressures of about 20 GPa [74,75]. While to the best of our knowledge there are no data in the literature for Ga_2Te_3, there has been a recent report that a closely related Ga_2SeTe_2 compound amorphizes under hydrostatic pressure [76]. These results suggest that relaxation of under-coordinated Te atoms (with LP orbitals) surrounding vacancies may be a common cause for both the pressure-induced amorphization and glasslike thermal conductivity. The high concentration of vacancies, enabling relatively large lattice relaxation, is likely to also be the underlying cause for easy amorphization of these materials upon exposure to intense laser or current pulses where a combination of electronic excitation and increased atomic vibrations due to temperature rise leads to destruction of the secondary bonds.

We now proceed to the amorphization process. In GST, once weaker secondary bonds are broken, the backbone covalent structure relaxes, leading to the formation of new bonds between threefold-coordinated Ge and Te atoms, a process that is accompanied by the formation of tetrahedral Ge sites and Ge-Ge bonds [8,38]. The latter serve to stabilize the amorphous phase. As proposed above, in Ga_2Te_3 after the destruction of the secondary Te-Te bonds the backbone structure also relaxes with the formation of like-atom bonds that preserve the stability of the amorphous phase. Our simulations suggest that the concentration of Te^2Te^4 pairs also increases in the amorphous phase.

A summary of the shared properties of GST and Ga_2Te_3 phase change materials is presented in Table II.

TABLE II. Summary of similar properties of $Ge_2Sb_2Te_5$ and Ga_2Te_3 materials [asterisk (*) indicates that pressure-induced amorphization was experimentally reported for a related Ga_2SeTe_2 compound].

Property
Crystalline phase
Metastable "cubic" phase (random vacancies)
Stable hexagonal phase (ordered vacancies)
High concentration of intrinsic vacancies
Dangling orbitals with LP electrons
Amorphous-like local distortions
Primary and secondary bonds
Glasslike thermal conductivity
Pressure-induced amorphization*
Amorphous phase
Increased band gap
Appearance of atoms with changed CN
Formation of "wrong' bonds"
High stability
Structure stabilization by over-coordinated atoms
Amorphization process
Destruction of secondary bonds
Preservation of the covalent backbone
Large optical contrast
High energy efficiency

IV. CONCLUSIONS

In conclusion, we have demonstrated that despite the zinc-blende average structure in the crystalline phase, Te atoms are locally (on average) threefold coordinated, with the resulting appearance of primary (Ga-Te) and secondary (Te-υ-Te) bonding. While the secondary Te-Te bonds across Ga vacancies cannot be called resonant, there is a clear similarity between Ga_2Te_3 and GST alloys in terms of the presence of two different kinds of bonds with a pronounced bonding energy hierarchy. We argue that similarly to the GST alloys, efficient switching in Ga_2Te_3 is due to the presence of primary and secondary bonding in the crystalline phase, whereas the structural stability of both phases is ensured by the polyvalency of Te atoms due to the presence of lone-pair electrons and also by the formation of like-atom bonds in the amorphous phase, by analogy with the GST alloys [17,38]. The bottom line of this work is that despite different crystal structures in GST and Ga_2Te_3, these materials share most of the attributes essential for highly efficient phase-change performance and possess a similar phase-change mechanism that is based on the reversible destruction/establishment of secondary bonds while preserving the covalent backbone structure.

ACKNOWLEDGMENTS

X-ray absorption studies were performed at BL01B1 of SPring-8 within the 2014B1257 proposal. M.K. also acknowledges Projects No. LM2015082 and No. CZ.1.05/4.1.00/11.0251 Center of Materials and Nanotechnologies co-financed by the European Fund of Regional Development and the state budget of the Czech Republic.

[1] S. R. Ovshinsky, Phys. Rev. Lett. **21**, 1450 (1968).
[2] T. Ohta and S. R. Ovshinsky, *Photo-Induced Metastability in Amorphous Semiconductors*, Chap. Phase-Change Optical Data Storage Media (Wiley-VCH, Weinheim, 2003), pp. 310–326.
[3] M. Wuttig and N. Yamada, Nat. Mater. **6**, 824 (2007).
[4] A. Kolobov, P. Fons, A. Frenkel, A. Ankudinov, J. Tominaga, and T. Uruga, Nat. Mater. **3**, 703 (2004).
[5] P. Jovari, I. Kaban, J. Steiner, B. Beuneu, A. Schops, and M. A. Webb, Phys. Rev. B **77**, 035202 (2008).
[6] D. A. Baker, M. A. Paesler, G. Lucovsky, S. C. Agarwal, and P. C. Taylor, Phys. Rev. Lett. **96**, 255501 (2006).
[7] S. Kohara, K. Kato, S. Kimura, H. Tanaka, T. Usuki, K. Suzuya, H. Tanaka, Y. Moritomo, T. Matsunaga, N. Yamada *et al.*, Appl. Phys. Lett. **89**, 201910 (2006).
[8] S. Caravati, M. Bernasconi, T. D. Kühne, M. Krack, and M. Parrinello, Appl. Phys. Lett. **91**, 171906 (2007).
[9] J. Akola and R. O. Jones, Phys. Rev. B **76**, 235201 (2007).
[10] J. Hegedüs and S. Elliott, Nat. Mater. **7**, 399 (2008).
[11] N. F. Mott, Adv. Phys. **16**, 49 (1967).
[12] M. Krbal, A. V. Kolobov, P. Fons, J. Tominaga, S. R. Elliott, J. Hegedus, and T. Uruga, Phys. Rev. B **83**, 054203 (2011).
[13] N. Yamada and T. Matsunaga, J. Appl. Phys. **88**, 7020 (2000).
[14] T. Matsunaga, R. Kojima, N. Yamada, K. Kifune, Y. Kubota, Y. Tabata, and M. Takata, Inorg. Chem. **45**, 2235 (2006).
[15] M. Wuttig, D. Lüsebrink, D. Wamwangi, W. Welnic, M. Gillessen, and R. Dronskowski, Nat. Mater. **6**, 122 (2007).
[16] G. Lucovsky and R. White, Phys. Rev. B **8**, 660 (1973).
[17] K. Shportko, S. Kremers, M. Woda, D. Lencer, J. Robertson, and M. Wuttig, Nat. Mater. **7**, 653 (2008).
[18] M. Ridgway, G. Azevedo, C. Glover, K. Yu, and G. Foran, Nucl. Instrum. Methods Phys. Res., Sect. B **199**, 235 (2003).
[19] A. V. Kolobov, M. Krbal, P. Fons, J. Tominaga, and T. Uruga, Nat. Chem. **3**, 311 (2011).
[20] M. Luo and M. Wuttig, Adv. Mater. **16**, 439 (2004).
[21] H. Zhu, J. Yin, Y. Xia, and Z. Liu, Appl. Phys. Lett. **97**, 083504 (2010).
[22] K. Kurosaki, H. Matsumoto, A. Charoenphakdee, S. Yamanaka, M. Ishimaru, and Y. Hirotsu, Appl. Phys. Lett. **93**, 012101 (2008).
[23] Y. Saito, Y. Sutou, and J. Koike, Appl. Phys. Lett. **102**, 051910 (2013).
[24] J. Skelton, K. Kobayashi, Y. Sutou, and S. Elliott, Appl. Phys. Lett. **102**, 224105 (2013).
[25] M. Popescu, F. Sava, A. Lőrinczi, A. Velea, I. Simandan, A. Galca, E. Matei, G. Socol, F. Gherendi, D. Savastru *et al.*, Phys. Status Solidi B **253**, 1033 (2016).
[26] G.-Y. Huang, N. Abdul-Jabbar, and B. Wirth, Acta Mater. **71**, 349 (2014).
[27] B. Ravel and M. Newville, J. Synchrotron Radiat. **12**, 537 (2005).
[28] J. J. Rehr, J. J. Kas, F. D. Vila, M. P. Prange, and K. Jorissen, Phys. Chem. Chem. Phys. **12**, 5503 (2010).
[29] G. Kresse and J. Hafner, Phys. Rev. B **47**, 558 (1993).
[30] G. Kresse and J. Furthmuller, Comput. Mater. Sci. **6**, 15 (1996).
[31] G. Kresse and J. Furthmuller, Phys. Rev. B **54**, 11169 (1996).
[32] G. Kresse and D. Joubert, Phys. Rev. B **59**, 1758 (1999).
[33] J. P. Perdew, J. A. Chevary, S. H. Vosko, K. A. Jackson, M. R. Pederson, D. J. Singh, and C. Fiolhais, Phys. Rev. B **46**, 6671 (1992).
[34] S. Clark, M. Segall, C. Pickard, P. Hasnip, M. Probert, K. Refson, and M. Payne, Z. Kristallogr. **220**, 567 (2005).
[35] A. J. Morris, R. J. Nicholls, C. J. Pickard, and J. R. Yates, Comput. Phys. Commun. **185**, 1477 (2014).
[36] A. Savin, R. Nesper, S. Wengert, and T. F. Fässler, Angew. Chem. Int. Ed. **36**, 1808 (1997).
[37] A. V. Kolobov, P. Fons, J. Tominaga, and S. R. Ovshinsky, Phys. Rev. B **87**, 165206 (2013).
[38] A. Kolobov, P. Fons, and J. Tominaga, Sci. Rep. **5**, 13698 (2015).
[39] M. Kastner, D. Adler, and H. Fritzsche, Phys. Rev. Lett. **37**, 1504 (1976).
[40] P. Newman and J. Cundall, Nature (London) **200**, 876 (1963).
[41] D. Singh, D. Suri, U. Dhawan, and K. Kundra, J. Mater. Sci. **25**, 2362 (1990).
[42] N. Abdul-Jabbar, T. Forrest, R. Gronsky, E. Bourret-Courchesne, and B. Wirth, J. Appl. Phys. **118**, 085707 (2015).
[43] G.-Y. Huang, N. Abdul-Jabbar, and B. Wirth, J. Phys.: Condens. Matter **25**, 225503 (2013).
[44] G. Dalba, D. Diop, P. Fornasini, and F. Rocca, J. Phys.: Condens. Matter **6**, 3599 (1994).
[45] S. Ahmed, G. Aquilanti, N. Novello, L. Olivi, R. Grisenti, and P. Fornasini, J. Chem. Phys. **139**, 164512 (2013).
[46] P. Becla, Z. Gumienny, J. Misiewicz, and J. Pawlikowski, Optica Applicata **12**, 143 (1982).
[47] S. Sajdlova, Ph.D. thesis, University of Pardubice, 2012.
[48] G. Harbeke and G. Lautz, Zeitschrift Naturforschung Teil A **11**, 1015 (1956).
[49] C. Julien, I. Ivanov, C. Ecrepont, and M. Guittard, Phys. Status Solidi A **145**, 207 (1994).
[50] S. Sen and D. Bose, Solid State Commun. **50**, 39 (1984).
[51] S. Ozaki, K. Takada, and S. Adachi, Jpn. J. Appl. Phys. **33**, 6213 (1994).
[52] A. Bekheet, Eur. Phys. J. Appl. Phys. **16**, 187 (2001).
[53] W. Welnic, S. Botti, L. Reining, and M. Wuttig, Phys. Rev. Lett. **98**, 236403 (2007).
[54] J. Robertson, K. Xiong, and P. W. Peacock, Thin Solid Films **515**, 7538 (2007).
[55] B. Huang and J. Robertson, Phys. Rev. B **81**, 081204(R) (2010).
[56] D. Singh and M. Khan, Indian J. Eng. Mater. Sci. **8**, 46 (2001).
[57] M. N. Schneider, P. Urban, A. Leineweber, M. Döblinger, and O. Oeckler, Phys. Rev. B **81**, 184102 (2010).
[58] T. Rosenthal, M. N. Schneider, C. Stiewe, M. Döblinger, and O. Oeckler, Chem. Mater. **23**, 4349 (2011).
[59] L. Shelimova, O. Karpinskii, M. Kretova, V. Kosyakov, V. Shestakov, V. Zemskov, and F. Kuznetsov, Inorg. Mater. **36**, 768 (2000).
[60] P. Nath and K. L. Chopra, Phys. Rev. B **10**, 3412 (1974).
[61] J. R. Sootsman, R. J. Pcionek, H. Kong, C. Uher, and M. G. Kanatzidis, Chem. Mater. **18**, 4993 (2006).
[62] H.-K. Lyeo, D. G. Cahill, B.-S. Lee, J. R. Abelson, M.-H. Kwon, K.-B. Kim, S. G. Bishop, and B. K. Cheong, Appl. Phys. Lett. **89**, 151904 (2006).
[63] J. P. Reifenberg, K.-W. Chang, M. A. Panzer, S. Kim, J. A. Rowlette, M. Asheghi, H.-S. Wong, and K. E. Goodson, IEEE Electron Device Lett. **31**, 56 (2010).
[64] E.-R. Sittner, K. S. Siegert, P. Jost, C. Schlockermann, F. R. L. Lange, and M. Wuttig, Phys. Status Solidi A **210**, 147 (2013).

[65] K. S. Siegert, F. R. L. Lange, E. R. Sittner, H. Volker, C. Schlockermann, T. Siegrist, and M. Wuttig, Rep. Prog. Phys. **78**, 013001 (2014).
[66] F. R. L. Lange, K. S. Siegert, and M. Wuttig, in *Frontiers of Electronic Materials*, edited by J. Heber, D. Schlom, Y. Tokura, R. Waser, and M. Wuttig (John Wiley & Sons, Weinheim, 2013).
[67] G. A. Slack, J. Phys. Chem. Solids **34**, 321 (1973).
[68] D. Spitzer, J. Phys. Chem. Solids **31**, 19 (1970).
[69] M. Beekman, D. T. Morelli, and G. S. Nolas, Nat. Mater. **14**, 1182 (2015).
[70] E. J. Skoug and D. T. Morelli, Phys. Rev. Lett. **107**, 235901 (2011).
[71] M. D. Nielsen, V. Ozolins, and J. P. Heremans, Energy Env. Sci. **6**, 570 (2013).
[72] M. Krbal, A. V. Kolobov, J. Haines, P. Fons, C. Levelut, R. Le Parc, M. Hanfland, J. Tominaga, A. Pradel, and M. Ribes, Phys. Rev. Lett. **103**, 115502 (2009).
[73] S. Caravati, M. Bernasconi, T. D. Kühne, M. Krack, and M. Parrinello, Phys. Rev. Lett. **102**, 205502 (2009).
[74] R. S. Kumar, A. L. Cornelius, E. Kim, Y. Shen, S. Yoneda, C. Chen, and M. F. Nicol, Phys. Rev. B **72**, 060101 (2005).
[75] A. V. Kolobov, J. Haines, A. Pradel, M. Ribes, P. Fons, J. Tominaga, Y. Katayama, T. Hammouda, and T. Uruga, Phys. Rev. Lett. **97**, 035701 (2006).
[76] N. Abdul-Jabbar, B. Kalkan, G.-Y. Huang, A. MacDowell, R. Gronsky, E. Bourret-Courchesne, and B. Wirth, Appl. Phys. Lett. **105**, 051908 (2014).